

# Quantitative analysis of H-species in anisotropic minerals by polarized infrared spectroscopy along three orthogonal directions

Kang Shuai<sup>1</sup> · Xiaozhi Yang<sup>1</sup>

Received: 6 September 2016 / Accepted: 6 February 2017 / Published online: 27 February 2017  
© Springer-Verlag Berlin Heidelberg 2017

**Abstract** Infrared spectroscopy is a powerful technique for probing H-species in nominally anhydrous minerals, and a particular goal of considerable efforts has been providing a simple yet accurate method for the quantification. The available methods, with either polarized or unpolarized analyses, are usually time-consuming or, in some cases, subjected to larger uncertainty than theoretically expected. It is shown here that an empirical approach for measuring the concentration, by determining three polarized infrared spectra along any three mutually perpendicular directions, is theoretically and in particular experimentally correct. The theoretical background is established by considering the integrated absorbance, and the experimental measurements are based on a careful evaluation of the species and content of H in a series of gem-quality orthogonal, monoclinic and triclinic crystals, including olivine, orthopyroxene, clinopyroxene, orthoclase and albite (natural and H-annealed). The results demonstrate that the sum of the integrated absorbance from two polarized spectra along two perpendicular directions in any given plane is a constant, and that the sum of the integrated absorbance from three polarized spectra along any three orthogonal directions is of essentially the same accuracy as that along the principal axes. It is also shown that this method works well, with a relative accuracy within 10%, even at some extreme cases where the sample absorption bands are both intense and strongly anisotropic.

**Keywords** Nominally anhydrous minerals · Infrared spectroscopy · H-species · Quantitative analysis · Polarized light

## Introduction

Over the past two decades, hydrogen, or more commonly water, dissolved in the lattice structure of nominally anhydrous minerals has received increasing attention, as a result of the widespread recognition of the importance of these assemblages as the dominant water reservoir in Earth's interior (e.g., Bell and Rossman 1992). The presence of hydrogen in the mineral structure is widely interpreted as H-related point defects such as OH groups, through charge-balanced substitutions (Keppler and Smyth 2006; and references therein), although it has been recently shown that molecular hydrogen, H<sub>2</sub>, can also be dissolved under reducing conditions (e.g., in the modern deep mantle and in the early Earth) by occupying interstitial positions (Yang et al. 2016). Such water, even in trace amounts, has a strong influence on many physicochemical properties of the host minerals and also key geochemical, geophysical and geodynamical processes of the Earth, including partial melting, electrical conductivity, rheological strength, plate tectonics and exchange of water between Earth's interior and exterior (e.g., Inoue 1994; Mei and Kohlstedt 2000; Regenauer-Lieb et al. 2001; Wang et al. 2006; Hirschmann and Kohlstedt 2012; Yang 2012a; Yang et al. 2014a). The effect of hydrogen on these various aspects, as well as the partitioning, distribution and storage of water inside the Earth, is closely related to its concentration levels, the types of its occurrence and the way it gets incorporated: e.g., the formation of OH defects could largely modify the silicate matrix of the host structure by breaking strong Si–O bond and/or by

Communicated by Jochen Hoefs.

✉ Xiaozhi Yang  
xzyang@nju.edu.cn

<sup>1</sup> State Key Laboratory for Mineral Deposits Research, School of Earth Sciences and Engineering, Nanjing University, Nanjing 210023, People's Republic of China

creating vacancies. Consequently, knowledge of the species and amount of hydrogen in nominally anhydrous minerals is of crucial importance.

Fourier-transform infrared (FTIR) spectroscopy was the first method established to determine hydrogen in nominally anhydrous minerals, and remains the most widely used one, despite the significant development of other techniques in recent years such as ion microprobe and elastic recoil detection analysis which measure the bulk content of all H-species. The main advantages include: (1) it is extremely sensitive to hydrogen, with detection limit down to the ppb level; (2) it distinguishes readily different types of H-species, such as OH groups, molecular H<sub>2</sub>O in inclusions and organic hydrogen as residues from sample preparation; (3) the analysis is easy, fast and inexpensive, and can be routinely conducted in situ on very small sample domains; (4) using polarized analyses, information on the orientations of H-species in the crystal structure and on the lengths of hydrogen bond can be deduced; and (5) given an externally determined calibration coefficient which is mineral dependent, the exact amount of H-species can be easily obtained from the measured spectra. Actually, a particular goal of considerable effort in the community in the past decades has been developing a simple but accurate method for measuring the concentration of hydrogen in nominally anhydrous minerals with FTIR spectroscopy, using either polarized or unpolarized radiation (e.g., Dowty 1978; Paterson 1982; Libowitzky and Rossman 1996; Asimow et al. 2006; Kovács et al. 2008; Sambridge et al. 2008; Withers 2013). However, most nominally anhydrous minerals are optically anisotropic. This makes the quantification with the available methods (in particular by polarized analyses) difficult and time-consuming, or sometimes, the results are potentially subjected to relatively large uncertainty (see the “Background” section).

An empirical approach, which has been adopted in some available reports (e.g., Johnson and Rossman 2003, 2004; Yang 2012a, b, 2015, 2016; Hamada et al. 2013; Yang et al. 2014b; Mosenfelder et al. 2015; Li et al. 2016), is that the concentrations of H-species in nominally anhydrous minerals can be determined from three mutually perpendicular polarized FTIR spectra of unoriented crystals. However, the validity of this theory has not been seriously evaluated, and some preliminary data on this issue in two recent studies have resulted in contrasting conclusions (Johnson and Rossman 2003; Mosenfelder et al. 2015; see also below). In this work, we have carried out a careful test to this method, by evaluating the basic theory and then conducting a systematic measurement of H-species in a series of orthogonal, monoclinic and triclinic minerals by FTIR spectroscopy, including olivine, orthopyroxene, clinopyroxene, orthoclase and albite, and the main focus is the experimental test. The results demonstrate that, for a given crystal

of a reasonable size (required for sample preparation), the H-content can be accurately measured by polarized FTIR analyses along any three orthogonal directions.

## Background

Quantitatively, the general principle for determining the abundance of H-species in silicate minerals by FTIR spectroscopy can be described by the modified version of the Beer–Lambert law:

$$C_{\text{water}} = \text{Abs}_{\text{total}}/I, \quad (1)$$

where  $C_{\text{water}}$  is the content of H-species, expressed as moles H<sub>2</sub>O/L mineral,  $\text{Abs}_{\text{total}}$  is the total integrated absorbance of H-related absorption bands in the region of interest normalized to 1 cm thickness (cm<sup>-2</sup>, e.g., by dividing the integrated area, cm<sup>-1</sup>, by the path thickness, cm), and  $I$  is the integral molar absorption coefficient (L mol<sup>-1</sup> cm<sup>-2</sup>). In most cases, the concentration is expressed as the equivalent content of H<sub>2</sub>O, ppm H<sub>2</sub>O (by weight), and the absorption coefficient is then the integral mineral-specific absorption coefficient ( $I'$ , ppm<sup>-1</sup> cm<sup>-2</sup>). As such, the most important is the accurate measurement of  $\text{Abs}_{\text{total}}$ , given that a reliable calibration coefficient is available. Concerning optically anisotropic minerals, the determined intensity of structural H-species depends strongly on the orientation of the infrared-active dipole relative to the incident radiation, and  $\text{Abs}_{\text{total}}$  is in principle the sum of the thickness-normalized integrated polarized absorbances along the three principal optical axes ( $X$ ,  $Y$  and  $Z$ ):

$$\text{Abs}_{\text{total}} = \text{Abs}_X + \text{Abs}_Y + \text{Abs}_Z. \quad (2)$$

This requires orienting single crystals along some basic planes, e.g., perpendicular to certain principal axes, so that the three optical axes can be determined. However, performing such a procedure on small grains, either natural or synthetic crystals, is usually time-consuming and very difficult, and the challenge is even greater for minerals with low symmetry, e.g., for some monoclinic or triclinic crystals of which axes are not always perpendicular to some fundamental planes.

In an attempt to avoid the preparation of oriented samples, Dowty (1978) and Libowitzky and Rossman (1996) theoretically proposed that, by polarized analyses, the  $\text{Abs}_{\text{total}}$  can be obtained by measurements of six vibration directions on any three orthogonal planes. This was examined by FTIR determinations with one topaz sample (Libowitzky and Rossman 1996). It should be noted that the study of Libowitzky and Rossman (1996) was actually on linear absorbance, which cannot be directly applied to integrated absorbance (Kovács et al. 2008; Sambridge et al. 2008; Withers 2013). Then, Asimow et al. (2006)

developed a method using polarized analyses on randomly oriented crystals, which are used to synthesize the three principal-axis spectra from a series of determinations, but information on the orientation of the analyzed grains is still required, e.g., by considering the silicate overtones. Measurements by unpolarized FTIR analyses have also been employed. Paterson (1982) initially introduced the concept of the orientation factor that allows an approximation of the  $Abs_{total}$  from analyses along a single direction with unpolarized (or polarized) radiation, but the relative uncertainty could be ~30–50% or even larger. In subsequent studies, it has been suggested that, in principle, unpolarized measurements on a statistically meaningful number of grains, e.g., ~10 to even more, of random orientations could yield the  $Abs_{total}$  of useful accuracy, within 10–30% (Kovács et al. 2008; Sambridge et al. 2008; Withers 2013). This requires the preparation of a polished thin section only, which is easier than the more demanding polarized analyses. However, a critical requirement of this approach is that the involved grains are of the same hydrogen content, which is also required by other methods involving multi-grains for the same sample (such as the one by Asimow et al. (2006)). In addition, it is stated clearly by those authors that this method is a good approximation if the H-related absorption bands are not very intense, with the linear polarized maximum absorbance  $<0.3$ , or moderately to weakly anisotropic, with similar maximum and minimum absorbance. A potential problem of this method is that crystals in many natural and synthetic samples are not randomly oriented, instead they are usually characterized by variable extent of lattice-preferred orientation (LPO: e.g., Karato 2008). This would lead to larger uncertainty than theoretically expected.

Empirically, the  $Abs_{total}$  of an anisotropic mineral crystal may be determined from polarized FTIR analyses along any three mutually perpendicular directions ( $X'$ ,  $Y'$  and  $Z'$ ), but not necessarily along the principal optical axes:

$$Abs_{total} = Abs_{X'} + Abs_{Y'} + Abs_{Z'} \quad (3)$$

Johnson and Rossman (2003) have done a simple test to this method with one anorthite sample (GRR 1968), and their measured  $Abs_{total}$  from three random but orthogonal directions agreed with that from the three optical axes to within 5% relative. In a very recent test of this method by Mosenfelder et al. (2015), however, a re-examination of the sample GRR 1968 yielded >30% higher  $Abs_{total}$  from three random directions than from the three principal axes. The contrasting difference may have been caused by heterogeneity of hydrogen in the sample, mis-estimation of the sample absorbance or large uncertainty involved with this approach, as stated by

those authors. This suggests that a systematic and careful experimental evaluation of Eq. (3) is still lacking. Moreover, a reasonable conclusion about the validity of the method may not be reached by examining only one or just a few samples.

The theory of Eq. (3) can be understood by considering some available work and the fundamentals of mathematics. In a given plane (e.g., a polished section) of an anisotropic crystal of a reasonable thickness, the integrated absorbance of a spectrum,  $Abs(\theta)$ , can be described by:

$$Abs(\theta) = Abs_{max} \cos^2(\theta - \phi) + Abs_{min} \sin^2(\theta - \phi), \quad (4)$$

where  $\theta$  is the polarization angle with respect to the reference direction (e.g., parallel to certain optical axis),  $Abs_{max}$  and  $Abs_{min}$  are the maximum and minimum integrated absorbance of the absorber in the plane, and  $\phi$  reflects the angle of the major axis of the combined function to the reference direction. This has been documented by Kovács et al. (2008), although it is pointed out by them that the linear absorbance form of Eq. (4) may be correct only if the linear polarized maximum absorbance is relatively small or the ratio of maximum and minimum absorbance is close to unity. For the integrated absorbance of two spectra from two perpendicular directions in the plane, we can easily obtain:

$$Abs(\theta) + Abs(\theta + 90^\circ) = Abs_{max} + Abs_{min} \quad (5)$$

This means that, for a given plane, the sum of the integrated absorbance of polarized spectra along any two perpendicular directions should be a constant. This can be extended to three-dimensional coordinate system that the  $Abs_{total}$  from polarized analyses along any three mutually perpendicular directions is also a constant (see Appendix), thus supporting Eq. (3). Note that the equivalent forms of Eqs. (4) and (5) about linear absorbance have already been mentioned by Libowitzky and Rossman (1996), although their focus was on other aspects as noted above.

We want to emphasize that Eqs. (4) and (5) may theoretically work only under some conditions, since the validity of their linear forms has some critical requirements and assumptions as noted above and elsewhere (Kovács et al. 2008; Sambridge et al. 2008; Withers 2013). The deduction of such equations requires the integral of some relations that do not have any analytical solutions (Kovács et al. 2008; Sambridge et al. 2008; Withers 2013), so that further evaluation of the involved theoretical background is not straightforward. However, the focus of this study is the experimental test below, and it does show that the method, concerning Eqs. (3)–(5), works excellently for a wide range of both sample thicknesses and spectral absorbance properties.

## Samples and methods

Samples for the measurements are some representative orthorhombic, monoclinic and triclinic crystals of gem quality, including olivine, orthopyroxene, clinopyroxene, orthoclase and albite. A brief description of the single crystals, natural and experimentally H-annealed, is given in Table 1. Dimensions of the starting natural crystals are ~10–60 mm. Chemical composition is homogeneous for each sample, as demonstrated by electron microprobe measurements, and the average data of representative samples are present in Table 2. Natural samples were from several different localities, with some examined also by Raman spectroscopy (Renishaw RM2000) and X-ray powder diffraction (Rigaku D/MAX RAPID II) for the phase identification, and starting materials for the H-annealing at elevated conditions were single crystal olivine from Liaohe (China, with <1 ppm H<sub>2</sub>O), orthopyroxene from Mpwa–Mpwa (Tanzania, with ~44 ppm H<sub>2</sub>O) and albite from Pingwu (China, with ~98 ppm H<sub>2</sub>O). The crystals were oriented by an X-ray precession camera for olivine and orthopyroxene and by morphology and cleavage for clinopyroxene, orthoclase and albite; in case of crystals

where only the orientation of one principal optical axis could be conveniently identified (e.g., some low-symmetry minerals), the other two orientations were determined by examining the two extinction directions in a plane perpendicular to this axis under an optical microscope. Uncertainty of the orientations is usually within  $\pm 5^\circ$  (Kerr 1977).

Blocks of  $\sim 1 \times 1.3 \times 1.6$  mm, with edges parallel to the three principal optical axes, respectively, were manufactured from the starting crystals, and were then loaded into capsules made of Ni or Pt, together with mineral fine powder surrounding the blocks as pressure media, Ni–NiO oxygen buffer and distilled water (corresponding to a bulk content of ~3–7%). Ni capsules were mechanically sealed upon compression, and Pt capsules were sealed by arc welding. H-annealing experiments were carried out at 1–3 GPa and 800–1300 °C with an end-loaded piston-cylinder press at the School of Earth Sciences and Engineering, Nanjing University and at 7 GPa and 1100 °C with a 1200 ton Kawai-type multi-anvil apparatus at the Bayerisches Geoinstitut. Run durations were typically 6.5–67 h depending on temperature (Table 1). Temperature was controlled by S- and D-type thermocouples for the piston-cylinder and multi-anvil runs, respectively. At the end of each experiment, the sample was quenched to room temperature by powering off the heating circuit, and the pressure was slowly released over 10–28 h to minimize crystal fracturing.

The samples showed no change in chemical composition during the experiments (Table 2). The recovered crystals, as well as machined small pieces of the H-bearing natural crystals which were not subjected to H-annealing, were double-polished along two perpendicular planes, which are parallel to one and two of the optical axes (*X*, *Y* and *Z*), respectively, and polarized FTIR analyses were subsequently carried out. The crystals were then double-polished again along two random but perpendicular planes, followed again by polarized FTIR analyses, and sometimes, this was repeated several times. In general, the polishing was applied to a single crystal of each sample (Fig. 1), and the orientation of the two perpendicular planes can be chosen arbitrarily, e.g., along or not along the principal axes. Then, two perpendicular polarized spectra were measured in one of these planes, and the third polarized spectrum was determined in the second plane, with polarized direction perpendicular to the intersecting edge of the two planes and thus normal to the first plane. By this, polarized spectra along the principal axes and along three random but mutually perpendicular directions could be obtained, with the electric field vector (*E*) parallel to these various directions. Thicknesses of the crystals, measured using a Mitutoyo digital micrometer, for FTIR analyses were usually ~100–800  $\mu\text{m}$ , but some samples were up to ~4 mm thick, e.g., the orthopyroxene sample (opx-1) for examining the

**Table 1** Sample description and water content

Sample <sup>#</sup>	Sample description	ppm H <sub>2</sub> O (by wt.)
oli-0	7 GPa, 1100 °C, 22 h, Ni–NiO	436
oli-1	1 GPa, 900 °C, 72 h, Ni–NiO	23
oli-3	1 GPa, 1200 °C, 9.5 h, Ni–NiO	70
oli-5	2 GPa, 1100 °C, 22 h, Ni–NiO	81
oli-6	1 GPa, 1100 °C, 23.5 h, Ni–NiO	61
oli-8	3 GPa, 1300 °C, 6.5 h, Ni–NiO	162
opx-1	Mpwa–Mpwa, Tanzania	44
opx-2	2.5 GPa, 1200 °C, 20 h, Ni–NiO	129
opx-3	3.5 GPa, 1200 °C, 20 h, Ni–NiO	165
cpx-1	Aksu, China	44
ort-1	Rhonegletscher, Switzerland	240
ort-4	Peshawar, Pakistan	678*
alb-1	Pingwu, China	98
alb-2	1 GPa, 800 °C, 67 h, Ni–NiO	168
alb-3	Taquaral, Brazil	9
alb-4	Pingwu, China	72

opx-1 and alb-1 were used as the starting materials for the H-annealing experiments of orthopyroxene (opx-2 and opx-3) and albite (alb-2), respectively

<sup>#</sup>oli olivine, opx orthopyroxene, cpx clinopyroxene, ort orthoclase, alb albite, (sample abbreviations are the same throughout this paper)

\*Reported as ppm NH<sub>4</sub><sup>+</sup> (by wt.). The small band at  $\sim 3625$  cm<sup>-1</sup>, due probably to molecular H<sub>2</sub>O (see text), was included for estimating the content; however, the band is very small (Fig. 3f) and thus contributes less to the bulk value

**Table 2** Chemical composition of representative samples by electron microprobe

Sample	SiO <sub>2</sub>	TiO <sub>2</sub>	Al <sub>2</sub> O <sub>3</sub>	FeO	MnO	MgO	CaO	Na <sub>2</sub> O	K <sub>2</sub> O	Total
Natural crystals										
Olivine	40.15	0.01	0.01	8.32	0.16	51.31	0.03	<0.01	<0.01	100.00
	<i>0.29</i>	<i>0.01</i>	<i>&lt;0.01</i>	<i>0.28</i>	<i>0.03</i>	<i>0.66</i>	<i>0.03</i>	<i>&lt;0.01</i>	<i>&lt;0.01</i>	
opx-1	57.41	0.05	0.05	5.82	0.24	36.77	0.09	0.06	0.01	100.50
	<i>0.30</i>	<i>0.02</i>	<i>0.01</i>	<i>0.23</i>	<i>&lt;0.01</i>	<i>0.15</i>	<i>0.03</i>	<i>&lt;0.01</i>	<i>&lt;0.01</i>	
cpx-1	53.79	<0.01	0.20	2.33	0.12	16.92	25.74	<0.01	<0.01	99.41
	<i>0.01</i>	<i>&lt;0.01</i>	<i>0.05</i>	<i>0.34</i>	<i>0.06</i>	<i>0.38</i>	<i>0.16</i>	<i>0.12</i>	<i>&lt;0.01</i>	
ort-1	64.04	0.03	19.92	<0.01	0.01	<0.01	0.01	1.76	13.61	99.40
	<i>0.15</i>	<i>0.04</i>	<i>0.13</i>	<i>0.00</i>	<i>0.01</i>	<i>&lt;0.01</i>	<i>0.02</i>	<i>0.06</i>	<i>0.05</i>	
ort-4	63.56	<0.01	20.08	0.01	<0.01	<0.01	<0.01	1.57	14.16	99.38
	<i>0.06</i>	<i>&lt;0.01</i>	<i>0.15</i>	<i>0.02</i>	<i>&lt;0.01</i>	<i>&lt;0.01</i>	<i>&lt;0.01</i>	<i>0.07</i>	<i>0.06</i>	
alb-1	68.16	<0.01	20.61	<0.01	<0.01	0.01	0.02	10.68	0.17	99.65
	<i>0.29</i>	<i>0.01</i>	<i>0.01</i>	<i>0.02</i>	<i>&lt;0.01</i>	<i>0.02</i>	<i>0.02</i>	<i>0.26</i>	<i>0.01</i>	
alb-3	68.27	<0.01	20.73	0.02	<0.01	0.01	0.01	10.71	0.18	99.91
	<i>0.15</i>	<i>&lt;0.01</i>	<i>0.16</i>	<i>0.02</i>	<i>&lt;0.01</i>	<i>0.01</i>	<i>0.01</i>	<i>0.04</i>	<i>0.01</i>	
H-annealed crystals										
oli-0	39.97	0.01	0.01	8.50	0.14	51.27	0.02	<0.01	<0.01	99.92
	<i>0.25</i>	<i>&lt;0.01</i>	<i>&lt;0.01</i>	<i>0.26</i>	<i>0.03</i>	<i>0.06</i>	<i>0.01</i>	<i>&lt;0.01</i>	<i>&lt;0.01</i>	
oli-1	40.37	0.02	<0.01	8.41	0.11	51.90	0.05	0.02	0.01	100.89
	<i>0.11</i>	<i>0.01</i>	<i>&lt;0.01</i>	<i>0.27</i>	<i>0.01</i>	<i>0.26</i>	<i>0.02</i>	<i>0.01</i>	<i>&lt;0.01</i>	
oli-3	39.83	<0.01	<0.01	8.66	0.15	50.73	<0.01	0.03	<0.01	99.40
	<i>0.31</i>	<i>&lt;0.01</i>	<i>&lt;0.01</i>	<i>0.22</i>	<i>&lt;0.01</i>	<i>0.05</i>	<i>&lt;0.01</i>	<i>&lt;0.01</i>	<i>&lt;0.01</i>	
oli-5	40.05	0.01	<0.01	8.64	0.12	50.82	0.02	0.01	<0.01	99.67
	<i>&lt;0.01</i>	<i>0.01</i>	<i>&lt;0.01</i>	<i>0.15</i>	<i>0.01</i>	<i>0.45</i>	<i>&lt;0.01</i>	<i>0.01</i>	<i>&lt;0.01</i>	
oli-6	39.85	0.01	0.01	8.89	0.14	50.39	0.02	0.01	0.01	99.31
	<i>0.15</i>	<i>0.02</i>	<i>0.01</i>	<i>0.18</i>	<i>0.01</i>	<i>0.18</i>	<i>0.01</i>	<i>0.01</i>	<i>0.01</i>	
oli-8	39.94	<0.01	0.01	8.61	0.14	50.85	0.01	<0.01	<0.01	99.57
	<i>0.09</i>	<i>&lt;0.01</i>	<i>0.02</i>	<i>0.56</i>	<i>0.02</i>	<i>0.16</i>	<i>0.01</i>	<i>&lt;0.01</i>	<i>&lt;0.01</i>	
opx-2	57.53	0.01	0.05	6.13	0.25	36.39	0.09	0.04	0.01	100.49
	<i>0.16</i>	<i>0.02</i>	<i>0.06</i>	<i>0.06</i>	<i>0.02</i>	<i>0.22</i>	<i>0.01</i>	<i>0.02</i>	<i>&lt;0.01</i>	
opx-3	57.51	0.07	0.06	5.53	0.25	37.00	0.07	0.05	<0.01	100.54
	<i>0.88</i>	<i>0.04</i>	<i>0.31</i>	<i>0.11</i>	<i>0.03</i>	<i>0.59</i>	<i>0.14</i>	<i>0.01</i>	<i>0.01</i>	
alb-2	68.65	<0.01	20.64	<0.01	0.01	<0.01	0.03	10.98	0.27	100.58
	<i>0.22</i>	<i>&lt;0.01</i>	<i>0.11</i>	<i>&lt;0.01</i>	<i>&lt;0.01</i>	<i>&lt;0.01</i>	<i>0.01</i>	<i>0.17</i>	<i>0.00</i>	

All Fe is reported as FeO. Data in the italic are the standard deviation of multi-point analyses

dependence of the in-plane integrated absorbances on the intensity and anisotropy of the absorption bands (see below section).

Chemical analyses of the samples were conducted at the School of Earth Sciences and Engineering, Nanjing University. Mineral chemistry was determined with a JEOL 8100 electron microprobe. The operating conditions were 15 kV accelerating voltage, 20 nA beam current, 1 μm beam diameter, and counting time of 10 and 5 s for the peak and background, respectively. Natural minerals were used as the standards, and data were reduced with the ZAF procedure. Polarized spectra were recorded with a Bruker Vertex 70V FTIR spectrometer coupled with a Hyperion 2000 microscope. 128 scans were accumulated in transmission

mode for each spectrum with a global source, a KBr/Ge beam splitter, a mid-band MCT detector, a ZnSe wire-grid polarizer, an aperture size of ~60×60 μm and a resolution of 4 cm<sup>-1</sup>. The polarizer was mounted in a Bruker rotatable polarizer mount, so that a particular degree of angle of polarized light could be chosen. Optically clean and inclusion- or fracture-free areas were chosen for the analyses. During the measurements, the optics of the spectrometer were always kept under vacuum, and the optics of the microscope were continuously purged by purified H<sub>2</sub>O- and CO<sub>2</sub>-free air. Baseline corrections of the spectra were performed with the commonly used spline-fit method (Appendix). Several reasonable baseline fittings were applied to a few representative spectra. The relative arbitrary

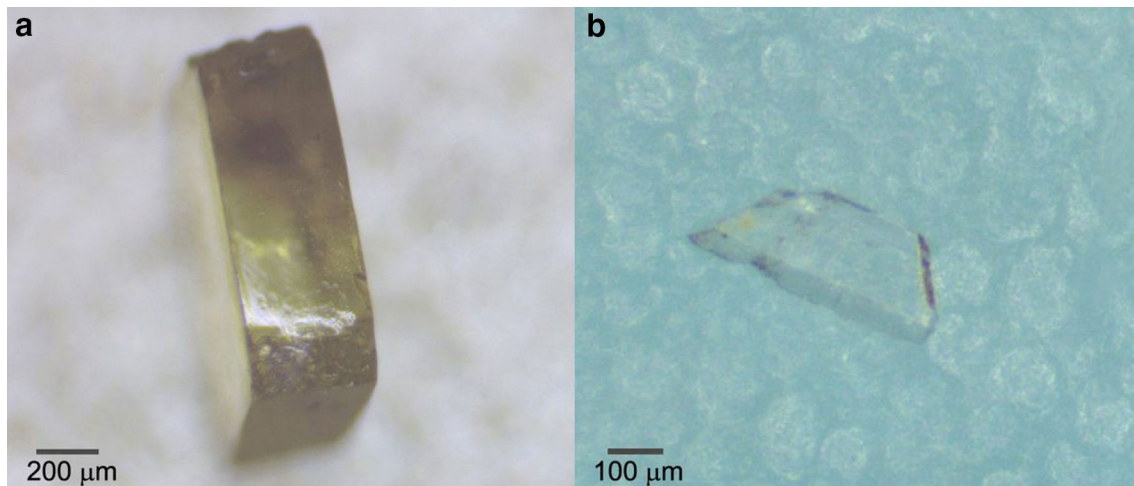


**Fig. 1** Representative polished single crystal of (a) oli-6 and (b) ort-4 for FTIR measurements. The olivine crystal in (a) was actually double-polished along three mutually perpendicular planes, with the section thickness of ~0.42, 0.91 and 0.85 mm, respectively, and the

orthoclase crystal in (b) was double-polished along two perpendicular planes, with the section thickness of ~0.07 and 0.16 mm, respectively. The crystals were slightly tilted for taking the photos

uncertainty due to manual fitting was commonly <5% for most of the spectra, and was <10% for some slightly noisy spectra. Hydrogen concentrations of the samples, by considering the polarized spectra along the three optical axes, were calibrated with the available mineral-specific absorption coefficients, as reported for OH in olivine by Bell et al. (2003), for OH in orthopyroxene and clinopyroxene by Bell et al. (1995), for OH and H<sub>2</sub>O in feldspars by Mosenfelder et al. (2015), and for NH<sub>4</sub><sup>+</sup> in feldspars by Solomon and Rossman (1988), and are shown in Table 1. It should, however, be mentioned that our results, discussion and conclusion are based on the calculated integrated absorbance, thus independent of the exact water content values and the calibration coefficients. Although we were very careful during sample preparations and FTIR measurements, uncertainty to the integrated absorbance from thickness determinations of the polished crystals and polarized analyses along different directions cannot be completely ruled out for at least individual samples. The relative contribution from these sources should be very little, e.g., a few percent at most, and the main uncertainty was from the spectral baseline corrections.

## Results and discussion

Profile FTIR analyses were conducted to all the crystals, and no zoned hydrogen distribution was detected on sub-grain scales (Fig. 2). In general, the samples all demonstrate H-related absorption bands in the mid-IR range ~3700–2700 cm<sup>-1</sup>. The calculated hydrogen contents range from ~9 to 439 ppm H<sub>2</sub>O plus a value of ~678 ppm

NH<sub>4</sub><sup>+</sup> in the ort-4 orthoclase (Table 1). Representative FTIR spectra are shown in Figs. 3 and 4, and the integrated absorbance values are present in Tables 3 and 4.

### H-species in samples

Orthorhombic crystals. Absorption bands centered at ~3612, 3597, 3573, 3566, 3544, 3523, 3483, 3448, 3411, 3393, 3353, 3326, 3219 and 3181 cm<sup>-1</sup> are observed for all the olivines H-annealed at 1–7 GPa and 900–1300 °C, and the bands at both high (~3700–3450 cm<sup>-1</sup>) and low (~3450–3100 cm<sup>-1</sup>) frequency are always evident, being much weaker with *E//Y* (Figs. 2a, 3a, 4a). These are typical OH groups reported for some mantle olivines (e.g., Matsuyuk and Langer 2004) and H-annealed Fe-bearing olivines (Demouchy and Mackwell 2006; Yang and Keppler 2011; Yang 2012a, 2015, 2016; Yang et al. 2014b). The natural orthopyroxene shows three dominant absorption bands at ~3513, 3411 and 3063 cm<sup>-1</sup>, and the band at ~3513 cm<sup>-1</sup> is the most significant, which is most intense with *E//Z* (Fig. 3b). In contrast, the two H-annealed orthopyroxenes are characterized by profound absorption bands at ~3685, 3600, 3544, 3513, 3415 and 3075 cm<sup>-1</sup>, and the bands differ greatly from those of the starting crystal, by especially the occurrence of a new sharp band at ~3600 cm<sup>-1</sup> (most intense with *E//Y*), the broadened band at ~3415 cm<sup>-1</sup> (most intense with *E//X*) and the greatly weakened band at ~3513 cm<sup>-1</sup> (Fig. 3c). These bands are similar to OH groups observed in natural and H-annealed Fe-bearing orthopyroxenes (e.g., Skogby et al. 1990; Rauch and Keppler 2002; Yang et al. 2016). The similar features of the OH bands, as found for H-annealed orthopyroxenes starting

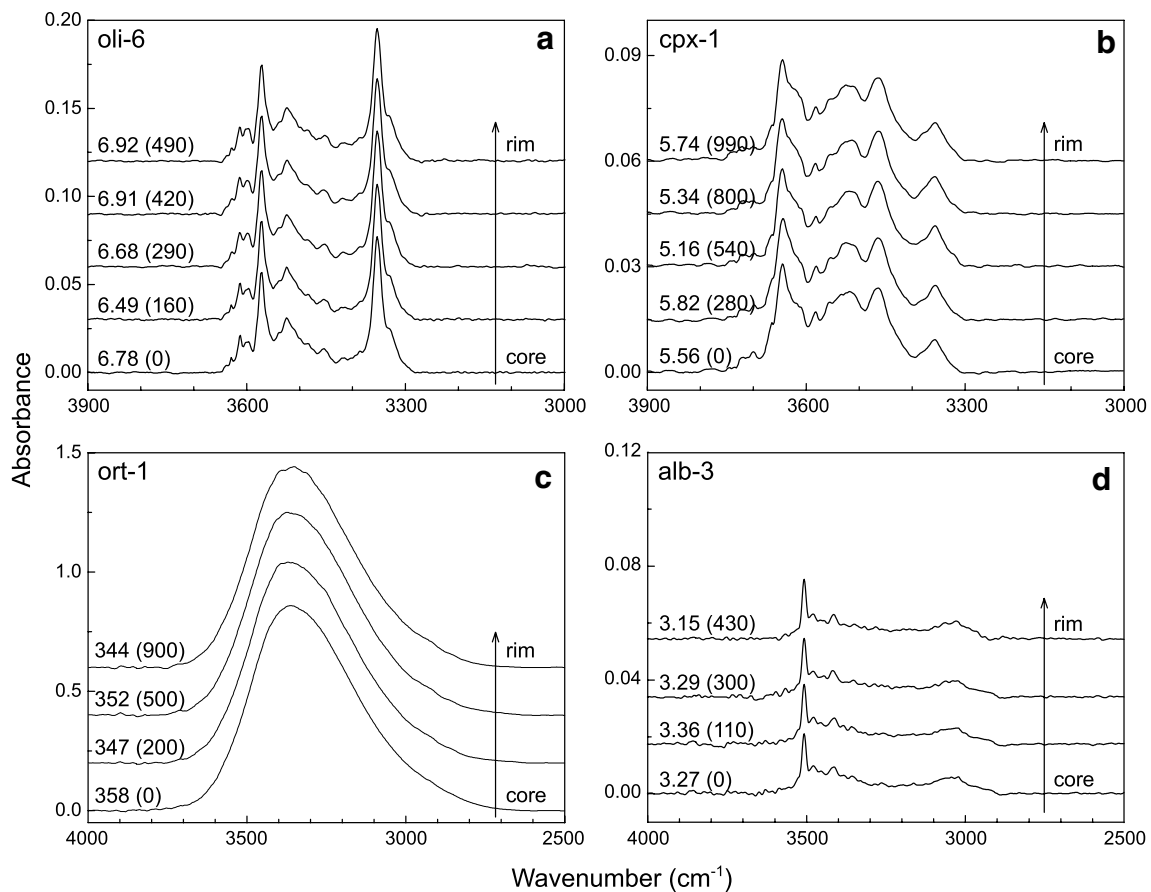


**Fig. 2** Profile FTIR spectra of H-species in representative samples. The spectra were normalized to 1 cm thickness and vertically offset. Numbers above each spectrum show the integrated absorbance ( $\text{cm}^{-2}$ ,

with an uncertainty of <10% relative, mostly <5%, due to baseline correction) and the estimated distance from crystal center ( $\mu\text{m}$  in parentheses, with an uncertainty of  $\sim 30\mu\text{m}$ )

with crystals also from Tanzania and the difference between them (Rauch and Keppeler 2002; Yang et al. 2016), suggest different types and populations of OH defects between the natural and H-annealed crystals.

**Monoclinic crystals.** The spectra of the clinopyroxene sample are dominated by absorption bands at  $\sim 3645$ ,  $3552$ ,  $3521$ ,  $3463$  and  $3355\text{ cm}^{-1}$  (Figs. 2b, 3d, 4b). These bands are typical for OH groups in natural diopside (e.g., Skogby et al. 1990). The band at  $\sim 3646\text{ cm}^{-1}$  is intense with  $E//X$  and  $E//Y$ , while the other bands are most intense with  $E//Z$ . Concerning the two orthoclase samples, distinctively different absorption bands are resolved between their spectra. For one orthoclase (ort-1), the spectra are dominated by broad and asymmetric bands at  $\sim 3360$  and  $3050\text{ cm}^{-1}$ : the former is intense with  $E//X$  and  $E//Z$ , while the latter is most intense with  $E//Y$  (Fig. 3e). According to Johnson and Rossman (2004), these bands are produced by OH groups. For the other orthoclase (ort-4), the spectra show a series of absorption bands between  $3700$  and  $2700\text{ cm}^{-1}$ , and the bands that can be readily resolved are at  $\sim 3625$ ,  $3463$ ,  $3295$ ,  $3251$ ,  $3216$ ,  $3070$  and  $2845\text{ cm}^{-1}$ ;

the small band at  $\sim 3625\text{ cm}^{-1}$  is most intense with  $E//X$ , and the other bands seem to show no significant pleochroism behaviors, although it should be mentioned that the one at  $\sim 3251\text{ cm}^{-1}$  appears more intense with  $E//X$  (Fig. 3f). Based on available survey of H-species in feldspars (Solomon and Rossman 1988; Johnson and Rossman 2004), the band at  $\sim 3625\text{ cm}^{-1}$  may be due to molecular  $\text{H}_2\text{O}$ , and the other bands can be reasonably attributed to  $\text{NH}_4^+$  structurally bound in the lattice.

**Triclinic crystals.** For the four albites, two different types of absorption patterns are identified. Three samples (alb-1, alb-2 and alb-4) demonstrate similar broad bands at  $3600\text{--}2700\text{ cm}^{-1}$ : the spectra with  $E//X$  are nearly symmetric, with the band centered at  $\sim 3230\text{ cm}^{-1}$ , and the spectra with  $E//Y$  and  $E//Z$  are asymmetric, with bands centered at  $3400\text{--}3200\text{ cm}^{-1}$  plus shoulder bands at lower frequencies (Fig. 3g). The similar bands between the starting alb-1 and the annealed alb-2, which is in contrast to the above mentioned orthopyroxenes, suggest that the H-annealing did not change the population of their H-defects, as experimentally documented for other feldspars (Yang 2012b).

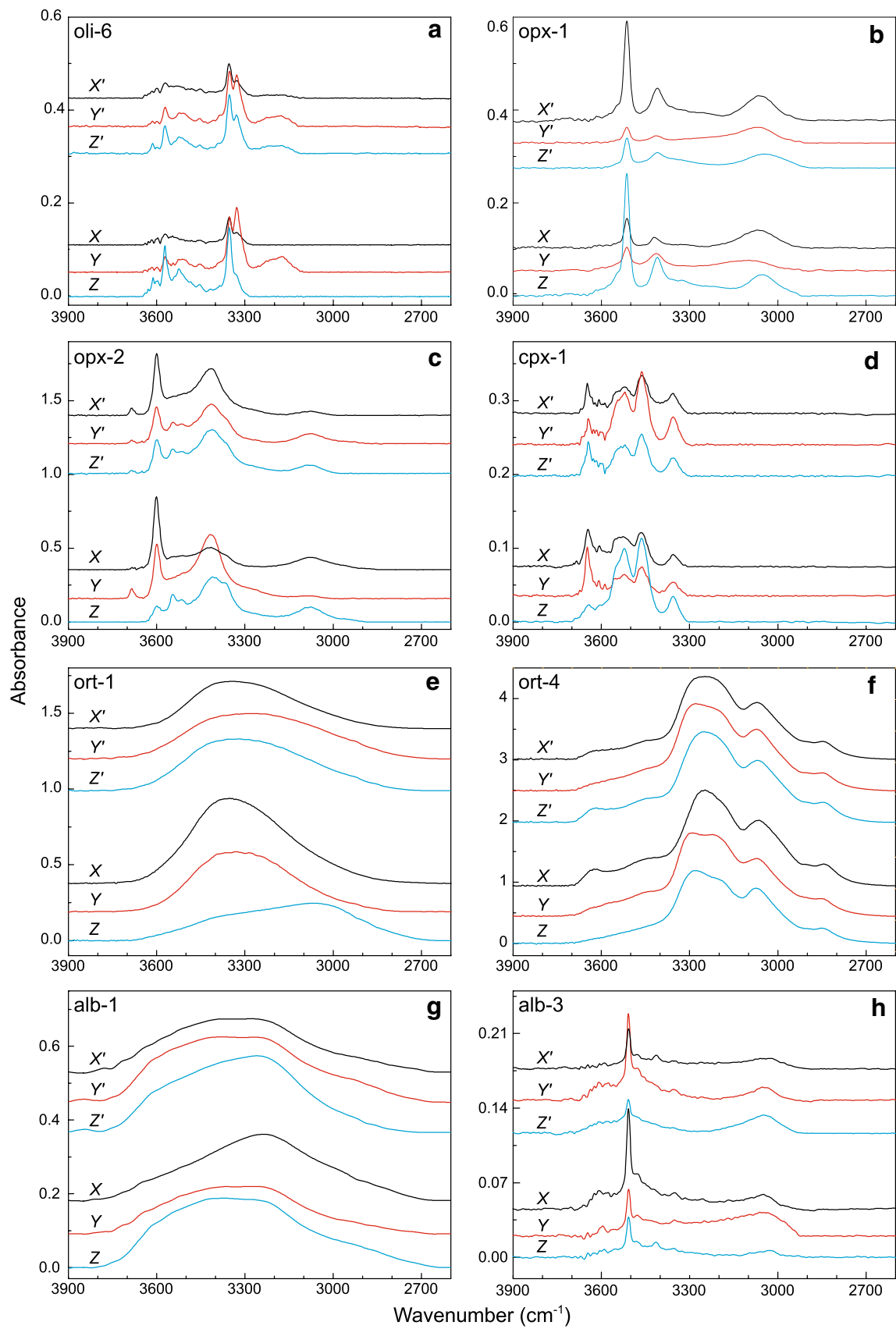




**Fig. 3** Polarized FTIR spectra of H-species in representative samples along the three principal optical axes ( $X$ ,  $Y$ , and  $Z$ ) and along any three orthogonal directions ( $X'$ ,  $Y'$  and  $Z'$ ). The spectra were normalized to 1 cm thickness and vertically offset. The bands at  $\sim 2845\text{ cm}^{-1}$  of the ort-4 sample (f) are still present after further polishing and cleaning, indicating that they cannot be due to residual organic H (e.g., crystal bond introduced during the sample preparation)

The bands differ distinctively from fluid inclusions which are characterized by broad and isotropic bands centered at  $\sim 3450\text{ cm}^{-1}$ , and are also different from the already identified types of OH groups in albites (Johnson and Rossman 2004). In addition, the spectra show weak bands at  $\sim 3640\text{ cm}^{-1}$ . Considering the results of Johnson and Rossman (2004), these bands may be caused either by the stretching of certain new type of OH groups in feldspars or by the occurrence of both molecular  $\text{H}_2\text{O}$  and OH groups in the structure. The assignment of the bands may need further work, but this does not influence our results about the quantification. The spectra of the other albite (alb-3) are different, and are dominated by broad bands centered at  $\sim 3100\text{--}3000\text{ cm}^{-1}$  and several small sharp bands at  $\sim 3600\text{--}3400\text{ cm}^{-1}$ , which appear most intense with  $E//X$  (especially for the most significant band at  $\sim 3507\text{ cm}^{-1}$ ; Fig. 3h). These bands are due to OH groups as reported for some natural and H-annealed albites (Johnson and Rossman 2004; Yang 2012b).

Regardless of the samples, the spectra measured along the three principal axes ( $X$ ,  $Y$  and  $Z$ ) and along any three orthogonal directions ( $X'$ ,  $Y'$  and  $Z'$ ) produce essentially the same defect types of H-species, regarding the frequency and number of the absorption bands, and the only difference is the relative intensity of individual bands, which is, as commonly known, sensitive to the infrared beam direction with respect to the orientations of anisotropic crystals (Fig. 3). As such, oriented crystals are actually not necessary for detecting the possible defect types, or H-sites, in a mineral, and the analyses by polarized FTIR measurements along any three mutually perpendicular directions are able to resolve all the absorption bands involved. Note that, in some classic studies, information about the species and patterns of hydrogen in some minerals is obtained even by unpolarized FTIR analyses on unoriented grains (e.g., Berry et al. 2005).

### Quantification of H-species and application

For any given plane, the shape of the polarized spectra usually evolves strongly with the polarization angle,  $\theta$  (Fig. 4), and so does the integrated absorbance,  $\text{Abs}(\theta)$ , or the band intensity (Fig. 5a). The variation of the integrated absorbance at different  $\theta$  can be a factor of up to  $\sim 3$  (Fig. 5a; Table 3). However, the sum of the integrated absorbance of two polarized spectra from any two perpendicular

directions is always the same, by taking into consideration the analytical uncertainty (Fig. 5b, c). This provides an excellent experimental support to the validity of Eq. (5).

The calculated  $\text{Abs}_{\text{total}}$  of all the samples is highly variable, ranging from  $\sim 120$  to  $16,000\text{ cm}^{-2}$  (Table 4). For each sample, the integrated absorbance of the polarized spectra along different directions shows some variation, which can be a factor of up to  $\sim 3$  (Table 4). For any sample, however, the  $\text{Abs}_{\text{total}}$  determined from the polarized spectra along the three principal optical axes is virtually the same as that along any three orthogonal directions. Plots of these data are given in Fig. 6 for the different minerals, and in general, excellent linear correlations are produced with the slopes of  $\sim 1$ . This indicates that the  $\text{Abs}_{\text{total}}$  of H-species, and thus the content, in optically anisotropic minerals can be accurately measured using polarized analyses along any three random but mutually perpendicular directions, lending strong support to the validity of Eq. (3).

It should be tested whether and to what extent the limits stated by Kovács et al. (2008) and Withers (2013), concerning the linear absorbance issues involved with the deduction of Eq. (4) as mentioned above, would have any apparent influence. A series of additional FTIR measurements in the (010) plane of a relatively large orthopyroxene crystal cut from the opx-1 sample, over a range of thickness, have been undertaken. The axis-related spectra of this sample, with  $E//Y$  and  $E//Z$ , are characterized by very large difference between the linear polarized maximum and minimum absorbance, e.g., by a factor of  $\sim 5\text{--}10$  for the band at  $\sim 3513\text{ cm}^{-1}$  (in contrast to the theoretically required limit of  $\sim 1$ ), and the maximum absorbance of this band is  $\sim 0.4\text{--}0.8$  (in contrast to the theoretically required upper limit of 0.3) for a range of thickness, e.g., at  $\sim 1.53\text{--}3.73\text{ mm}$  (Figs. 3b, 7a). It turns out that the sum of the integrated absorbance from two perpendicular spectra is not a constant for the very thick samples at  $\sim 2.91\text{--}3.73\text{ mm}$ , with very high maximum absorbance of about  $0.7\text{--}0.8$  (Fig. 7a), and that the value is lower at  $\sim 45^\circ$  angular deviation from the reference axis (Fig. 7b). This in general agrees with the theoretical modeling for sample linear absorbance at comparable angular conditions (Sambridge et al. 2008). It should also be pointed out that, for FTIR measurements done on very thick samples with a microscope coupled to an FTIR spectrometer (e.g., up to  $\sim 4\text{ mm}$  here), the measured absorbance may deviate from the true value due to refraction of the uncollimated beam inside the sample. This is produced by the fact that the convergent radiation passes through the Cassegrainian objective at an angle, but not parallel to the surface of sample section and thus forms a truncated cone inside the section; the thicker the sample, the larger the cone. This would result in biased integrated absorbances for very thick

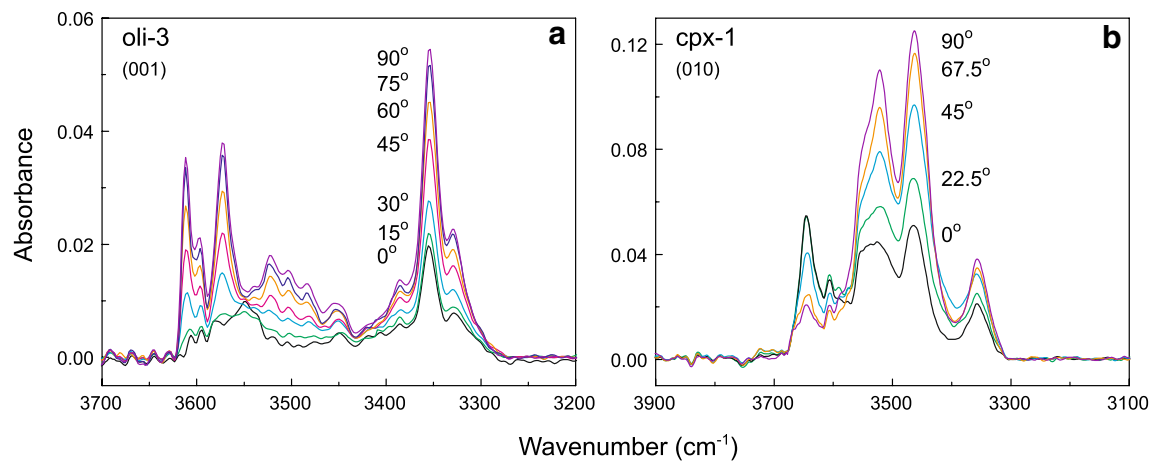


**Fig. 4** In-plane angular FTIR spectra of H-species in representative samples. **a** The spectra were taken in the (001) plane of oli-3, by a step of 15°, and the reference direction was parallel to *Y*, and **b** The spectra were taken in the (010) plane of cpx-1, by a step of 30°, and

the reference direction was parallel to *X*. The spectra were normalized to 1 cm thickness, and the polarization angle ( $\theta$ ) was shown for each spectrum

**Table 3** Angular variation of in-plane integrated absorbance of H-species

Sample	Abs( $\theta$ )/Abs( $\theta+90^\circ$ ) <sup>#</sup>								Abs( $\theta$ ) + Abs( $\theta+90^\circ$ )			
	90°	67.5°	45°	22.5°	0°	-22.5°	-45°	-67.5°	0°	22.5°	45°	67.5°
oli-0	726	670	761	857	1132	1053	1107	887	1858	1744	1868	1722
oli-1	20		17		53		51		73		68	
oli-5	127		149		167		142		294		291	
oli-6	49		76		130		77		180		154	
oli-8	140		179		314		262		454		441	
opx-1	263	207	129	111	115	157	202	262	378	373	331	364
opx-2	512	543	649	764	798	784	650	542	1310	1306	1299	1327
opx-3	636		734		906		837		1542		1571	
cpx-1	159	122	102	96	85	112	137	141	244	236	239	234
ort-1	1351	1331	1665	2097	2303	2414	1962	1636	3654	3733	3627	3745
ort-4	4599	4664	4776	5296	6071	5990	5416	4643	10,670	10,654	10,192	9938
alb-1	750	775	848	950	965	997	886	783	1715	1734	1733	1772
alb-2	1755	1920	2101	2225	2174	2130	2126	1795	3929	4020	4228	4049
alb-3	44		90		99		53		143		143	

$\theta$  is the polarization angle with respect to the reference direction (see text). Usually, the reference direction was taken as parallel to certain optical axis, but in some cases, it was taken as a random direction

<sup>#</sup>Pairs of integrated absorbance along two perpendicular directions

samples, as documented by Maldener et al. (2003). This may also contribute to the observed deviation of sample absorbance in Fig. 7, at ~3–4 mm thickness. However, our data demonstrate clearly that, even for these rather extreme conditions when the absorption bands are simultaneously intense and strongly anisotropic, the summed integrated band absorbance of any two perpendicular spectra is still consistent with each other within 10% relative (Fig. 7b). In particular, the variation of the summed integrated absorbance of any two perpendicular spectra of the sample at a thickness of ~2.03 mm,

where the difference between linear maximum and minimum absorbance is still very large (~0.67 vs. 0.03), is much smaller, e.g., within 5% relative (Fig. 7b). These, in combination with the excellent linear correlation between the summed integrated absorbance of the polarized spectra along the two axes (*Y* and *Z*) and the sample thickness (Fig. 7c), suggest that even at relatively extreme conditions, Eq. (5), and furthermore Eq. (3), is still valid with an accuracy within 10% relative. Such an uncertainty is actually at the same level of that involved with the baseline corrections of H-species in most, if not

**Table 4** Integrated absorbance of H-species along various directions

Sample	Principle optical axes				Three orthogonal directions <sup>#</sup>			
	Abs <sub>X</sub>	Abs <sub>Y</sub>	Abs <sub>Z</sub>	Abs <sub>total</sub>	Abs <sub>X'</sub>	Abs <sub>Y'</sub>	Abs <sub>Z'</sub>	Abs <sub>total</sub>
oli-0	1132	462	726	2320	595	1045	854	2494
					595	1096	709	2400
					1053	462	670	2184
					1107	462	761	2330
					887	462	857	2206
oli-1	53	20	52	125	32	49	43	125
					51	17	52	120
oli-3	170	54	163	387	80	142	135	357
					80	123	154	357
					77	151	163	391
					96	124	163	383
					114	112	163	390
					127	81	163	371
oli-5	167	127	139	433	170	160	125	456
					142	149	139	430
					79	130	131	340
oli-6	130	49	143	323	77	76	143	297
					77	76	143	297
oli-8	314	140	408	862	116	370	362	848
					262	179	408	849
					225	98	120	443
opx-1	115	111	263	489	157	111	207	475
					202	111	129	442
					262	111	111	484
					638	580	682	1901
opx-2	798	611	512	1921	784	611	543	1939
					650	611	649	1910
					542	611	764	1918
					958	891	693	2541
opx-3	926	636	906	2468	926	837	734	2497
					926	837	734	2497
cpx-1	159	70	85	314	85	132	90	307
					112	70	122	305
					137	70	102	309
					141	70	96	307
ort-1	2303	1351	1466	5120	1345	1879	1831	5055
					2414	1331	1466	5211
					1962	1665	1466	5093
					1636	2097	1466	5199
ort-4	6071	5499	4599	16,170	4600	5368	5917	15,884
					5990	5499	4664	16,154
					5416	5499	4776	15,691
					4643	5499	5296	15,438
alb-1	965	750	1162	2877	864	1105	1112	3081
					997	775	1162	2934
					886	848	1162	2895
					783	950	1162	2895
alb-2	2174	1755	980	4909	2127	1220	1119	4467
					2130	1920	980	5029
					2126	2101	980	5208

**Table 4** (continued)

Sample	Principle optical axes				Three orthogonal directions <sup>#</sup>			
	Abs <sub>X</sub>	Abs <sub>Y</sub>	Abs <sub>Z</sub>	Abs <sub>total</sub>	Abs <sub>X'</sub>	Abs <sub>Y'</sub>	Abs <sub>Z'</sub>	Abs <sub>total</sub>
alb-3	114	99	44	257	54	79	136	269
alb-4	697	723	676	2095	489	519	914	1922

<sup>#</sup>For some samples, polarized FTIR spectra and integrated absorbance were measured for several groups of three orthogonal directions (Fig. 6), but in some cases one direction was maintained the same (perpendicular to the plane where analyses along the other two directions were carried out, see Table 3)

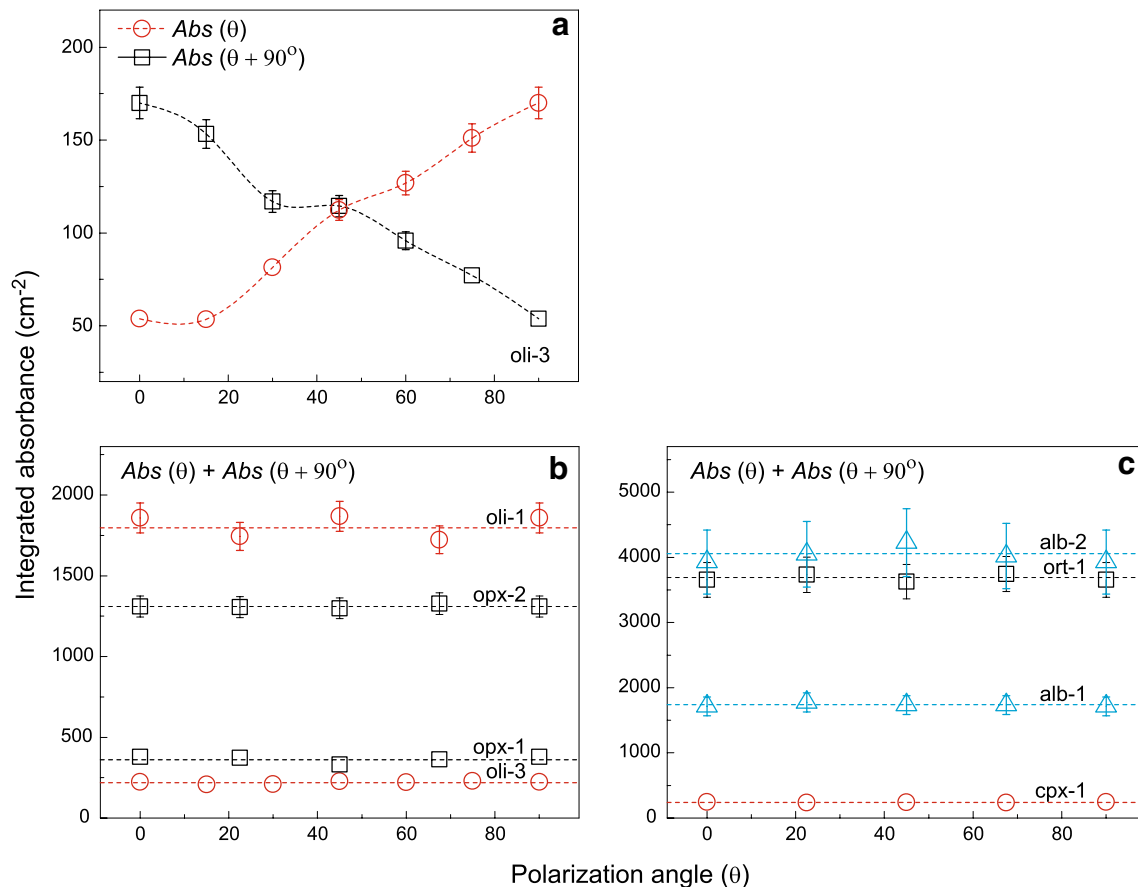


**Fig. 5** In-plane angular absorbance of H-species in representative samples. **a** The integrated absorbance along two perpendicular directions as a function of  $\theta$  for sample oli-3. **b** The sum of the integrated absorbance along two perpendicular directions as a function of  $\theta$  for orthorhombic olivine and orthopyroxene, and **c** The sum of the integrated absorbance along two perpendicular directions as a function

of  $\theta$  for monoclinic clinopyroxene and orthoclase and triclinic albite. All the values were normalized to 1-cm thickness. Dashed curves and lines are used for reference only. Error bars were assumed 5 or 10% relative (see text for details), which are in some cases smaller than the symbol size

all, FTIR spectra, either polarized or unpolarized. Thus, it appears that the quantification method under extreme absorbance conditions does not suffer significantly from the theoretically deduced technical limits as casted for unpolarized FTIR measurements (Kovács et al. 2008; Withers 2013).

### Comparison with other methods

The species and especially the total integrated absorbance (Abs<sub>total</sub>), and thus the content given a reliable calibration coefficient, of hydrogen in optically anisotropic nominally anhydrous minerals can be excellently determined by

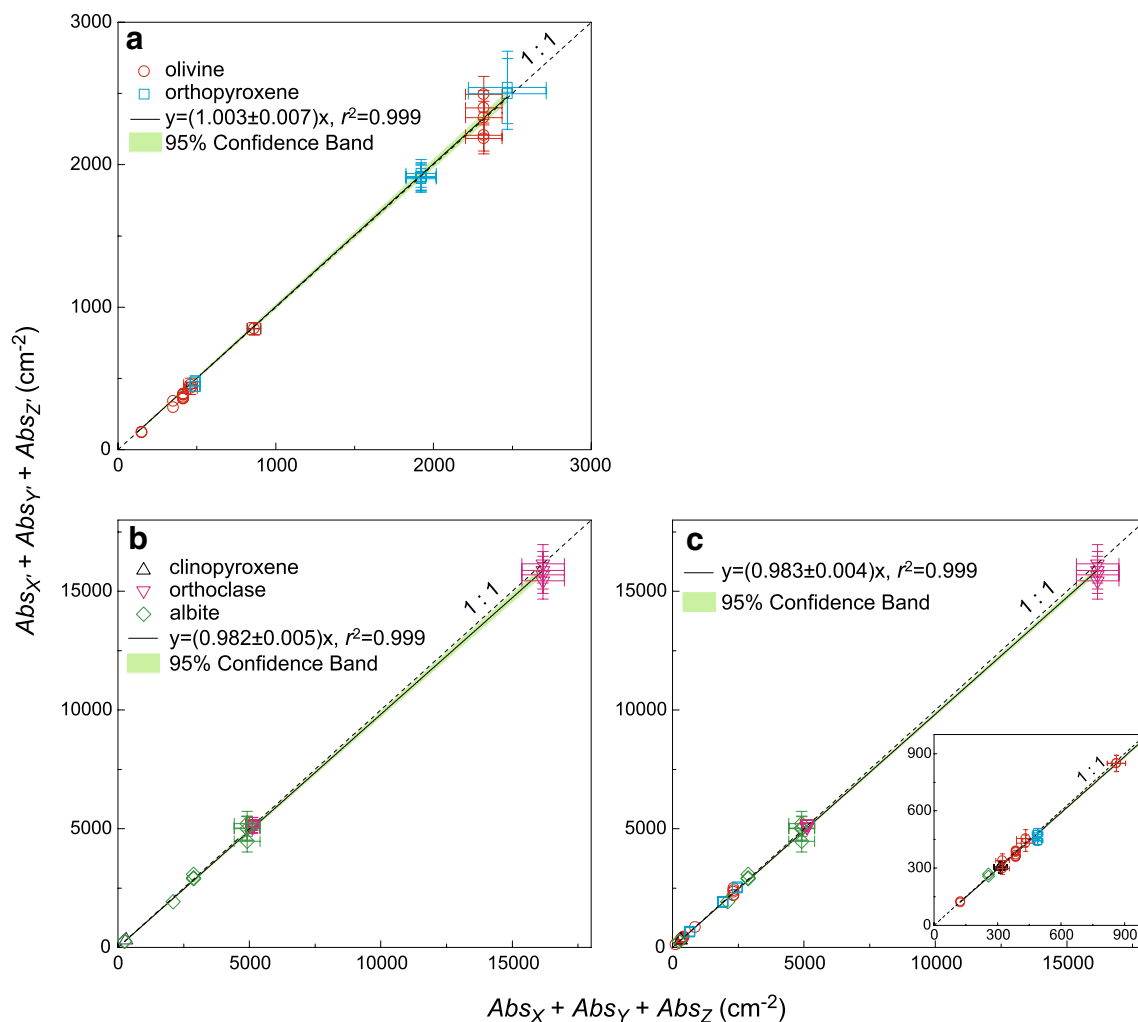


**Fig. 6** Plot of total integrated absorbance along the principal optical axes ( $X$ ,  $Y$ , and  $Z$ ) and along any three orthogonal directions ( $X'$ ,  $Y'$  and  $Z'$ ). **a** Orthorhombic olivine and orthopyroxene, with the least-square regression yielding a relation of  $(Abs_{X'} + Abs_{Y'} + Abs_{Z'}) = 1.003 (\pm 0.007) \times (Abs_X + Abs_Y + Abs_Z)$ ,  $r^2 = 0.999$ , **b** Monoclinic clinopyroxene + orthoclase and triclinic albite, with the least-square regression yielding a relation of  $(Abs_{X'} + Abs_{Y'} + Abs_{Z'}) = 0.982 (\pm 0.005) \times (Abs_X + Abs_Y + Abs_Z)$ ,  $r^2 = 0.999$ , and **c** All the samples shown in (a) and (b), with

the least-square regression of all the data yielding a relation of  $(Abs_{X'} + Abs_{Y'} + Abs_{Z'}) = 0.983 (\pm 0.004) \times (Abs_X + Abs_Y + Abs_Z)$ ,  $r^2 = 0.999$ . All the linear fittings, represented by *solid lines*, were forced to pass through the zero point. *Shadowed regions* illustrated the 95% confidence band of the fittings, and *dashed diagonal lines* show the 1:1 reference ratio. *Error bars* were assumed 5 or 10% relative (see text for details), which are in some cases smaller than the symbol size

measuring three polarized FTIR spectra along any three mutually perpendicular directions. The yielded accuracy is essentially the same as that of the standard method by determining three polarized spectra along the three principal axes. The method is not that sensitive to band linear absorbance and/or sample thickness, and the accuracy is within  $\sim 10\%$  relative even at some extreme conditions, e.g., for some very thick samples (up to  $\sim 4$  mm) with strong anisotropy in H-related absorption bands. In common studies on FTIR measurements of H-species in single crystal minerals, sample sections are usually prepared with a reasonable thickness, e.g.,  $< 1$  mm for most samples and  $< 100$   $\mu\text{m}$

for extremely H-rich samples such as H-abundant wadsleyite and ringwoodite, and this method can be safely applied.

In the past years, two FTIR-based approaches are frequently used for quantifying H-species in minerals. One is the standard polarized method, which requires oriented crystals and three polarized spectra along the three principal optical axes (e.g., Bell et al. 2003), and the other is the modified unpolarized method, which requires analyses on a population of unoriented crystals with random orientations (Kovács et al. 2008; Withers 2013). As noted above, the first is of high accuracy, yet the preparation of oriented samples is difficult and time-consuming; the

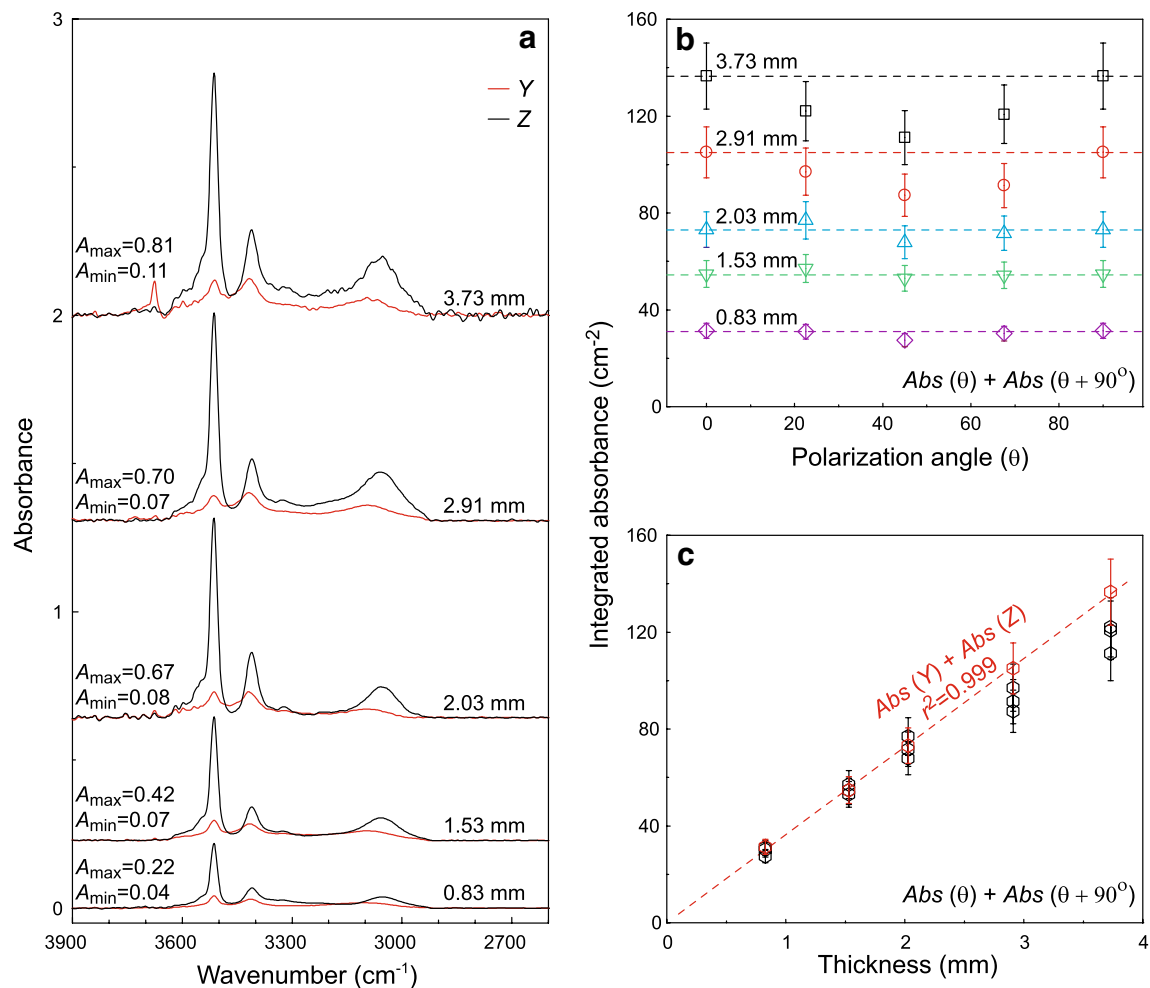


**Fig. 7** Thickness-related polarized FTIR measurements on the (010) plane of opx-1. **a** Polarized spectra with  $E//Y$  and  $E//Z$  as a function of thickness, **b** Sum of integrated absorbance along two perpendicular directions as a function of  $\theta$ , and **c** Sum of integrated absorbance from two perpendicular spectra as a function of thickness. The spectra and integrated absorbance were not thickness-normalized.  $A_{\max}$  and  $A_{\min}$  in **(a)** are the linear polarized maximum and minimum absorbance of the band at  $\sim 3671 \text{ cm}^{-1}$ , respectively. A small band

second involves simple procedure for sample preparation, but is less accurate and some critical requirements about the spectral absorbance properties must be satisfied. In comparison, the proposed approach is of some apparent advantages: (1) it allows to estimate the concentration of H-species in anisotropic minerals by polarized analyses in two arbitrarily chosen but perpendicular planes of a given crystal, and consideration of the sample orientation and the principal optical axes is not necessary; (2) it can be safely applied to samples with a wide range of spectral absorbance properties (e.g., it still works accurately even for minerals with intense and strongly anisotropic H-related bands), which resembles the standard polarized method and is a great merit over the unpolarized method; and (3) it

at  $\sim 3687 \text{ cm}^{-1}$ , similar to that in the H-annealed samples (Fig. 3c), is observed for the thickness of  $\sim 3.73 \text{ mm}$  **(a)**, indicating that the H-site is also present in natural orthopyroxene (but due to the very low intensity, this band can only be detected in very thick samples). The reference direction of the polarization angle was taken parallel to the axis  $Y$ . Dashed lines in **(b)** are for reference only, and dashed line in **(c)** is the least-square regression of the data for the two axes (red symbols), with the fitting forced to pass through the zero point

yields essentially the same accuracy, except for extremely thick samples which are actually not common for determining H content in practical studies, as the standard polarized method, and is in general more accurate than the unpolarized method.

Some potential issues involved with the application of this approach should be clarified. (1) grain-scale H distribution. To test the validity of this approach, samples that show no zoned H distribution within sub-grain scales were employed. To have a physically meaningful H-content, homogeneity of H-distribution in any samples must be first examined, e.g., by profile analyses. This is a prerequisite for the proposed approach, as required also by other FTIR methods including the standard polarized one and

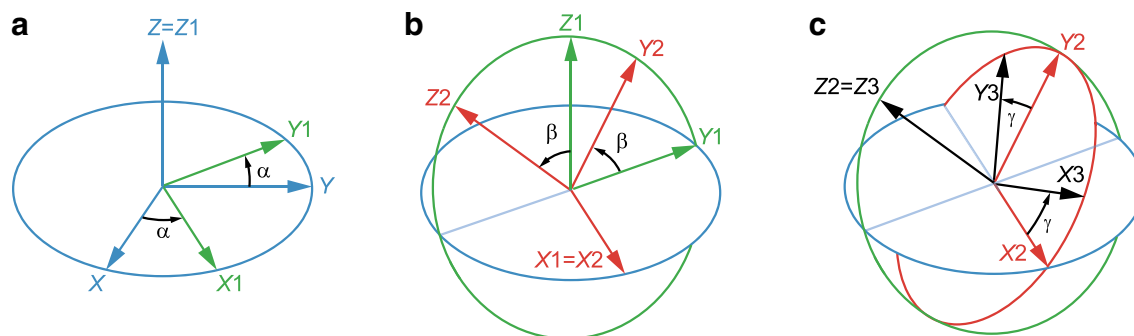


**Fig. 8** A  $z$ - $x$ - $z$  rotation of the three-dimensional coordinate system. **a** The first rotation around the  $Z$  axis, **b** The second rotation around the  $X1$  axis, and **c** The third rotation around the  $Z2$  axis.  $X1$ ,  $X2$ ,  $Y1$ ,  $Y2$ ,  $Z1$  and  $Z2$  are the axes after the first and second rotations.  $\alpha$ ,  $\beta$ ,

and  $\gamma$  are the Euler angles:  $\alpha$  represents a rotation around the  $Z$  axis,  $\beta$  represents a rotation around the  $X1$  axis, and  $\gamma$  represents a rotation around the  $Z2$  axis

the modified unpolarized one (although it should be noted that details about the H-homogeneity may vary between these methods, in particular for those involving one crystal vs. multi crystals for the quantification). (2) sample size. The proposed approach requires double-polishing of a single crystal sample along two perpendicular planes. Such a preparation procedure is easy and routinely achievable for relatively large crystals, e.g.,  $\sim 500\ \mu\text{m}$  to  $>1\ \text{mm}$ . However, this does not appear impossible for crystals as small as  $\sim 100$ – $200\ \mu\text{m}$ , according to this work (e.g., polished crystals in Fig. 1) and our previous experience (Yang 2012a, b, 2015, 2016; Yang et al. 2014b, 2016; Li et al. 2016). Mineral grains in natural xenolith, xenocryst or megacryst samples could be  $\sim 1$ – $2\ \text{mm}$  in size or even larger, except for extremely fine-grained samples from strongly deformed shear zones and very tiny mineral inclusions captured by some crystals, and experimentally synthesized samples, in particular those by H-annealing natural crystals, could also be up to  $\sim 1\ \text{mm}$  in size or larger (depending on run conditions and apparatus), although it should be noted that grains grown from hydrous melts at elevated  $P$ - $T$  conditions are usually a few to tens of  $\mu\text{m}$  in size. Therefore, many of these samples can be treated with the proposed approach for an accurate quantification of the H-species. For crystals of smaller sizes (e.g.,  $<100\ \mu\text{m}$ ), the preparation of polished samples would be challenging, and the approach could not work easily. This is caused by challenges involved with sample preparation but not by the method itself (note that the standard polarized method is confronted with the same difficulty if only one oriented single crystal is polished and analyzed for the three axis-related polarized spectra). (3) since the crystals are not oriented in the proposed approach, orientations of H-species in the lattice structure cannot be deduced (the same issue for other polarized or unpolarized methods on unoriented crystals). However, studies concerning the structural orientations of hydrogen in various minerals have been performed extensively elsewhere (e.g.,

Keppler and Smyth 2006; and references therein), and in particular, knowledge about the species and concentration of hydrogen in nominally anhydrous (and hydrous) minerals is in most cases, if not all, more important for evaluating the possible physicochemical influences.

**Acknowledgements** The H-annealing experiment of sample oli-0 at the Bayerisches Geoinstitut was done by X.Y. in 2011. Constructive comments by István Kovács and Jed Mosenfelder helped to improve the manuscript. This study was supported by the National Basic Research Program of China (2014CB845904), the National Science Foundation of China (41590622 and 41372041), and the Recruitment Program of Global Young Experts (P.R. China).

## Appendix

1. Equation (3) in the three-dimensional coordinate system.

Euler angles are used to describe the orientation of any reference frame (typically, a coordinate system or basis) as a composition of the three elemental rotations starting from a known standard orientation. To theoretically produce Eq. (3), the  $\text{Abs}_{\text{total}}$  determined from the polarized FTIR spectra along the three principal axes is the same as the one along any three mutually perpendicular directions, we adopt an approach by considering the Euler angles.

For simplicity, the three axes are labeled as  $X$ ,  $Y$  and  $Z$ , and the three orthogonal directions are labeled as  $X3$ ,  $Y3$  and  $Z3$  (Fig. 8). We consider the theory by imagining a rotation of the three-dimensional coordinate system. In general, any rotation can be achieved by six possibilities of choosing the rotation axes for proper Euler angles, and any orientation can be achieved by composing three elemental rotations. The following is taken with the  $z$ - $x$ - $z$  rotation as an example but can be applied to any other forms of rotation.

Let us assume a fixed H-bearing absorber. Initially, the total absorbance is  $\text{Abs}_{\text{total}} = \text{Abs}_X + \text{Abs}_Y + \text{Abs}_Z$  [Eq. (2)].

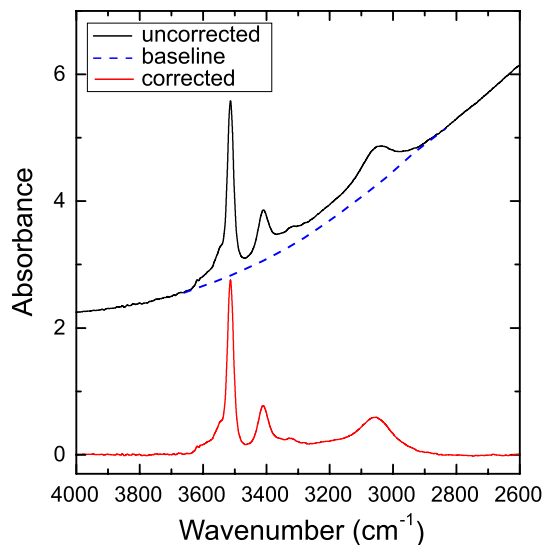


**Fig. 9** A representative spectrum for baseline correction. Uncorrected, baseline and corrected spectra shown by *black, blue and red lines*, respectively. The spectra are from opx-1 and were normalized to 1 cm thickness

Since for a given plane, the sum of the integrated absorbance from two perpendicular directions is a constant [Eq. (5)], we immediately have:

after the first rotation around the Z axis ( $Z=Z_1$ , Fig. 7a),  $Abs_x + Abs_y = Abs_{x_1} + Abs_{y_1}$ , so that  $Abs_{total} = Abs_{x_1} + Abs_{y_1} + Abs_{z_1}$ ;

after the second rotation around the X1 axis ( $X_1=X_2$ , Fig. 7b),  $Abs_{y_1} + Abs_{z_1} = Abs_{y_2} + Abs_{z_2}$ , so that  $Abs_{total} = Abs_{x_2} + Abs_{y_2} + Abs_{z_2}$ ;

after the third rotation around the Z2 axis ( $Z_2=Z_3$ , Fig. 7c),  $Abs_{x_2} + Abs_{y_2} = Abs_{x_3} + Abs_{y_3}$ , so that  $Abs_{total} = Abs_{x_3} + Abs_{y_3} + Abs_{z_3}$ .

This means that the  $Abs_{total}$  is indeed the sum of the integrated absorbance along any three orthogonal directions [Eq. (3)].

## 2. Baseline corrections.

Backgrounds of the spectra were corrected by the commonly used spline fit of the baseline defined by points outside the OH-stretching region, and a representative example is shown in Fig. 9.

## References

Asimow PD, Stein LC, Mosenfelder JL, Rossman GR (2006) Quantitative polarized infrared analysis of trace OH in populations of randomly oriented mineral grains. *Am Mineral* 91:278–284

Bell DR, Rossman GR (1992) Water in Earth's mantle: the role of nominally anhydrous minerals. *Science* 255:1391–1397

Bell DR, Ihinger PD, Rossman GR (1995) Quantitative analysis of trace OH in garnet and pyroxenes. *Am Mineral* 80:465–474

Bell DR, Rossman GR, Maldener J, Endisch D, Rauch F (2003) Hydroxide in olivine: a quantitative determination of the absolute amount and calibration of the IR spectrum. *J Geophys Res* 108:B22105 doi:10.1029/2001JB000679

Berry AJ, Hermann J, O'Neill HSC, Foran GJ (2005) Fingerprinting the water site in mantle olivine. *Geology* 33:869–872

Demouchy S, Mackwell S (2006) Mechanisms of hydrogen incorporation and diffusion in iron-bearing olivine. *Phys Chem Miner* 33: 347–355

Dowty E (1978) Absorption optics of low-symmetry crystals—application to titanian clinopyroxene spectra. *Phys Chem Miner* 3: 173–181

Hamada M, Ushioda M, Fujii T, Takahashi E (2013) Hydrogen concentration in plagioclase as a hygrometer of arc basaltic melts: approaches from melt inclusion analyses and hydrous melting experiments. *Earth Planet Sci Lett* 365:253–262

Hirschmann M, Kohlstedt DL (2012) Water in Earth's mantle. *Phys Today* 65: 40–45

Inoue T (1994) Effect of water on melting phase relations and melt composition in the  $Mg_2SiO_4$ - $MgSiO_3$ - $H_2O$  system up to 15 GPa. *Phys Earth Planet Inter* 85: 237–263

Johnson EA, Rossman GR (2003) The concentration and speciation of hydrogen in feldspars using FTIR and  $^1H$  MAS NMR spectroscopy. *Am Mineral* 88:901–911

Johnson EA, Rossman GR (2004) A survey of hydrous species and concentrations in igneous feldspars. *Am Mineral* 89:586–600

Karato S (2008) Deformation of earth materials: an introduction to the rheology of solid earth. Cambridge University Press, Cambridge

Keppeler H, Smyth JR (2006) Water in nominally anhydrous minerals. Mineralogical Society of America, Washington, pp. 478

Kerr PF (1977) Optical mineralogy. McGraw-Hill Book Company, Inc., New York

Kovács I, Hermann J, O'Neil HSC, Gerald JF, Sambridge M, Horvath G (2008) Quantitative absorbance spectroscopy with unpolarized light: Part II. experimental evaluation and development of a protocol for quantitative analysis of mineral IR spectra. *Am Mineral* 93:765–778

Li Y, Yang X, Yu JH, Cai YF (2016) Unusually high electrical conductivity of phlogopite: the possible role of fluorine and geophysical implications. *Contrib Mineral Petrol* 171:37. doi:10.1007/s00410-00016-01252-x

Libowitzky E, Rossman GR (1996) Principles of quantitative absorbance measurements in anisotropic crystals. *Phys Chem Miner* 23: 319–327

Maldener J, Hosch A, Langer K, Rauch F (2003) Hydrogen in some natural garnets studied by nuclear reaction analysis and vibrational spectroscopy. *Phys Chem Miner* 30: 337–344

Matsyuk SS, Langer K (2004) Hydroxyl in olivines from mantle xenoliths in kimberlites of the Siberian platform. *Contrib Mineral Petrol* 147:413–437

Mei S, Kohlstedt DL (2000) Influence of water on plastic deformation of olivine aggregates 2. dislocation creep regime. *J Geophys Res* 105:21471–21481

Mosenfelder JL, Rossman GR, Johnson EA (2015) Hydrous species in feldspars: a reassessment based on FTIR and SIMS. *Am Mineral* 100:1209–1221

Paterson MS (1982) The determination of hydroxyl by infrared absorption in quartz, silicate glasses and similar materials. *Bull Minéral* 105: 20–29

Rauch M, Keppeler H (2002) Water solubility in orthopyroxene. *Contrib Mineral Petrol* 143:525–536

Regenauer-Lieb K, Yuen DA, Branlund J (2001) The initiation of subduction: criticality by addition of water? *Science* 294:578–580

Sambridge M, Gerald JF, Kovács I, O'Neil HSC, Hermann J (2008) Quantitative absorbance spectroscopy with unpolarized light:



- Part I. physical and mathematical development. *Am Mineral* 93:751–764
- Skogby H, Bell DR, Rossman GR (1990) Hydroxide in pyroxene: variations in the natural environment. *Am Mineral* 75:764–774
- Solomon GC, Rossman GR (1988)  $\text{NH}_4^+$  in pegmatitic feldspars from the southern Black Hills, South Dakota. *Am Mineral* 73:818–821
- Wang D, Mookherjee M, Xu Y, Karato S (2006) The effect of water on the electrical conductivity of olivine. *Nature* 443:977–980
- Withers AC (2013) On the use of unpolarized infrared spectroscopy for quantitative analysis of absorbing species in birefringent crystals. *Am Mineral* 98:689–697
- Yang X (2012a) Orientation-related electrical conductivity of hydrous olivine, clinopyroxene and plagioclase and implications for the structure of the lower continental crust and uppermost mantle. *Earth Planet Sci Lett* 317–318:241–250
- Yang X (2012b) An experimental study of H solubility in feldspars: effect of composition, oxygen fugacity, temperature and pressure and implications for crustal processes. *Geochim Cosmochim Acta* 97:46–57
- Yang X (2015) OH solubility in olivine in the peridotite-COH system under reducing conditions and implications for water storage and hydrous melting in the reducing upper mantle. *Earth Planet Sci Lett* 432:199–209
- Yang X (2016) Effect of oxygen fugacity on OH dissolution in olivine under peridotite-saturated conditions: an experimental study at 1.5–7 GPa and 1100–1300 °C. *Geochim Cosmochim Acta* 173:319–336
- Yang X, Keppler H (2011) In-situ infrared spectra of OH in olivine to 1100 °C. *Am Mineral* 96:451–454
- Yang X, Keppler H, Dubrovinsky L, Kurnosov A (2014a) In-situ infrared spectra of hydroxyl in wadsleyite and ringwoodite at high pressure and high temperature. *Am Mineral* 99:724–729
- Yang X, Liu D, Xia Q (2014b)  $\text{CO}_2$ -induced small water solubility in olivine and implications for properties of the shallow mantle. *Earth Planet Sci Lett* 403:37–47
- Yang X, Keppler H, Li Y (2016) Molecular hydrogen in mantle minerals. *Geochem Perspect Lett* 2: 160–168